AGU PUBLICATIONS

Global Biogeochemical Cycles

RESEARCH ARTICLE
10.1002/2015GB005120

Key Points:
- Central Pacific mercury cycling is distinct from that in the North Pacific
- Organic matter remineralization alone does not predict mercury methylation
- Little mercury enrichment has occurred in Equatorial Pacific waters since 1990

Supporting Information:
- Figures S1 and S2
- Table S1

Correspondence to:
K. M. Munson,
kathleenmunson@gmail.com

Citation:
Munson, K. M., C. H. Lamborg, G. J. Swarr, and M. A. Saito (2015), Mercury species concentrations and fluxes in the Central Tropical Pacific Ocean, *Global Biogeochem. Cycles*, *29*, 656–676, doi:10.1002/2015GB005120.

Received 16 FEB 2015
Accepted 23 APR 2015
Accepted article online 25 APR 2015
Published online 25 MAY 2015

Mercury species concentrations and fluxes in the Central Tropical Pacific Ocean

Kathleen M. Munson[1,2], Carl H. Lamborg[1,3], Gretchen J. Swarr[1], and Mak A. Saito[1]

[1]Department of Marine Chemistry and Geochemistry, Woods Hole Oceanographic Institution, Woods Hole, Massachusetts, USA, [2]MIT/WHOI Joint Program in Chemical Oceanography, Woods Hole, Massachusetts, USA, [3]Now at Department of Ocean Sciences, University of California, Santa Cruz, California, USA

Abstract The formation of the toxic and bioaccumulating monomethylmercury (MMHg) in marine systems is poorly understood, due in part to sparse data from many ocean regions. We present dissolved mercury (Hg) speciation data from 10 stations in the North and South Equatorial Pacific spanning large water mass differences and gradients in oxygen utilization. We also compare the mercury content in suspended particles from six stations and sinking particles from three stations to constrain local Hg sources and sinks. Concentrations of total Hg (THg) and methylated Hg in the surface and intermediate waters of the Equatorial and South Pacific suggest Hg cycling distinct from that of the North Pacific gyre. Maximum concentrations of 180 fM for both MMHg and dimethylmercury (DMHg) are observed in the Equatorial Pacific. South of the equator, concentrations of MMHg and DMHg are less than 100 fM. Sinking fluxes of particulate THg can reasonably explain the shape of dissolved THg profiles, but those of MMHg are too low to account for dissolved MMHg profiles. However, methylated Hg species are lower than predicted from remineralization rates based on North Pacific data, consistent with limitation of methylation in Equatorial and South Pacific waters. Full water column depth profiles were also measured for the first time in these regions. Concentrations of THg are elevated in deep waters of the North Pacific, compared to those in the intermediate and surface waters, and taper off in the South Pacific. Comparisons with previous measurements from nearby regions suggest little enrichment of THg or MMHg over the past 20 years.

1. Introduction

Human exposure to the toxic element mercury (Hg) is linked to its chemical speciation in marine environments. Humans are primarily exposed to Hg in the bioaccumulating form, monomethylmercury (MMHg), through consumption of marine fish [*Food and Agriculture Organization of the United Nations*, 2013]. However, concentrations of MMHg compose <15% of total mercury (THg) in the water column of the Atlantic and Pacific Oceans [*Hammerschmidt and Bowman*, 2012; *Cossa et al.*, 2011; *Mason and Sullivan*, 1999; *Sunderland et al.*, 2009; *Mason and Fitzgerald*, 1991, 1993]. The majority of Hg in marine systems is in inorganic forms: Hg^{2+} complexed to organic ligands and dissolved gaseous elemental Hg (Hg^0). A fourth species, dissolved dimethylmercury (DMHg), which is largely unique to seawater, can also be found at significant concentrations but at less than <7% of THg [*Cossa et al.*, 1997; *Mason and Fitzgerald*, 1990, 1993; *Mason and Sullivan*, 1999; *Hammerschmidt and Bowman*, 2012].

Water column methylation of inorganic divalent Hg(II) has long been invoked to account for elevated MMHg and DMHg concentrations observed in the marine water column [*Mason and Fitzgerald*, 1990; *Cossa et al.*, 2009; *Sunderland et al.*, 2009]. Although resulting MMHg concentrations depend on the availability of the Hg(II) substrate for methylation, prediction of methylation is complicated by the redox chemistry of Hg(II), which drives cycling back and forth to Hg^0. As a result of its multiple identities in marine environments, the bioaccumulation of Hg in marine food webs and ultimate exposure of humans to Hg depends on its transformations between Hg pools.

Maximum MMHg concentrations in the open ocean water column are typically found at depths of net remineralization [*Mason and Fitzgerald*, 1993; *Mason and Sullivan*, 1999; *Laurier et al.*, 2004; *Cossa et al.*, 2009; *Sunderland et al.*, 2009; *Cossa et al.*, 2011; *Hammerschmidt and Bowman*, 2012]. However, the exact mechanism of marine MMHg production remains unclear. Water column MMHg maxima were first attributed to the water column production of MMHg from breakdown of photolabile DMHg, which was thought to be the direct product of Hg(II) methylation [*Mason and Fitzgerald*, 1993]. More recently, direct

production of MMHg from Hg(II) was found to dominate MMHg production in the Arctic water column [*Lehnherr et al*., 2011].

Understanding the mechanism of methylation has important implications for determining how MMHg concentrations change with time as a result of Hg loadings to the oceans. Recently, Pacific fish tissue has been found to carry isotopic signals of mass-independent fractionation attributed to photodemethylation as well as signals of mass-dependent fractionation attributed to methylation [*Blum et al*., 2013]. From the depth dependence of these isotopic signatures, *Blum et al*. [2013] estimate that the majority of MMHg incorporated into marine food webs originates below the surface mixed layer. Microbial methylation by a mechanism analogous to that known to occur in anaerobes [*Gilmour et al*., 2013] is one explanation for subsurface MMHg production [*Blum et al*., 2013]. However, to date, there have been no direct observations of methylation by water column marine microbes. The overlap between the isotopic signatures attributed to microbial methylation [*Rodriguez-Gonzalez et al*., 2009] and those of abiotic Hg methylation [*Jimenez-Moreno et al*., 2013] prevents a clear identification of the mechanism of marine methylation. As a result, due to the complexity of mass-dependent fractionation, attributing the observed fractionation signatures to a marine mechanism analagous to that of bacteria in anoxic environments may be premature.

In the absence of a mechanistic understanding of marine methylation, various biological indicators have been explored as potential controls on methylation. Based on the distributions of methylated Hg species, the relationship between net remineralization and methylation has been explored in several ocean basins. A weak ($r^2 = 0.20$) but positive correlation was observed between DMHg and apparent oxygen utilization (AOU) in waters from the upper 1500 m of the Equatorial and South Atlantic [*Mason and Sullivan*, 1999]. A much stronger relationship ($r^2 = 0.76$) was observed between total methylated Hg (MMHg + DMHg) and AOU in the Southern Ocean [*Cossa et al*., 2011]. The link between AOU and methylated Hg concentrations is strongest in young waters, such as the Mediterranean [*Cossa et al*., 2009]. To deconvolute the link between organic carbon remineralization and methylated Hg in older North Pacific waters, concentrations of methylated Hg were compared with the rate of organic matter remineralization [*Sunderland et al*., 2009]. In addition to the strong correlation observed in methylated Hg concentrations, the percentage of methylated Hg in North Pacific waters were elevated relative to surface waters, which indicated that methylation, rather than release of MMHg from particulate matter, was responsible for elevated concentrations in these waters [*Sunderland et al*., 2009].

Quantifying Hg speciation is critical for understanding its potential to enter marine food webs. However, measurements of all four dissolved Hg chemical species are limited to a few areas in the open ocean. *Mason and Fitzgerald* [1993] first measured MMHg and DMHg in the Equatorial Pacific. However, their relatively high detection limits of 50 fM resulted in measurable concentrations of MMHg in only ~30% of water depths analyzed [*Mason and Fitzgerald*, 1993]. *Hammerschmidt and Bowman* [2012] provided dissolved concentrations of MMHg, DMHg, and THg as well as particulate THg and MMHg at a single site in the North Pacific, with no values below their detection limit. That work notwithstanding, more recent efforts to determine sources of MMHg were hampered by analytical challenges in preserving Hg speciation. Due to its instability in acidic conditions, DMHg cannot be easily preserved for shore-based determination. As a result, studies of MMHg production have relied on total methylated Hg concentrations ([DMHg] + [MMHg]) [e.g., *Sunderland et al*., 2009; *Cossa et al*., 2011].

Data sets that include both dissolved and particulate Hg concentrations are also uncommon. No measurements of open ocean Hg species sinking fluxes have been published despite the potential such measurements have to quantify sources of dissolved MMHg. *Hammerschmidt and Bowman* [2012] observed increases in the ratio of particulate MMHg to particulate carbon with water column depth that they interpret as either the preferential retention of MMHg on particles, particle scavenging of MMHg in the water column, or production of MMHg on sinking particles.

A recent analysis of North Pacific water found that increased Asian emissions, roughly doubling over the past 25 years [*Pacyna et al*., 2006], have increased total Hg concentrations in the North Pacific Intermediate Waters (NPIWs) [*Sunderland et al*., 2009] compared to values measured in 1987 and 2002 [*Gill and Bruland*, 1987; *Laurier et al*., 2004]. However, no studies have yet revisited the Equatorial Pacific waters first measured by *Mason and Fitzgerald* [1993]. Our cruise track (Figure 1) extended from the southern

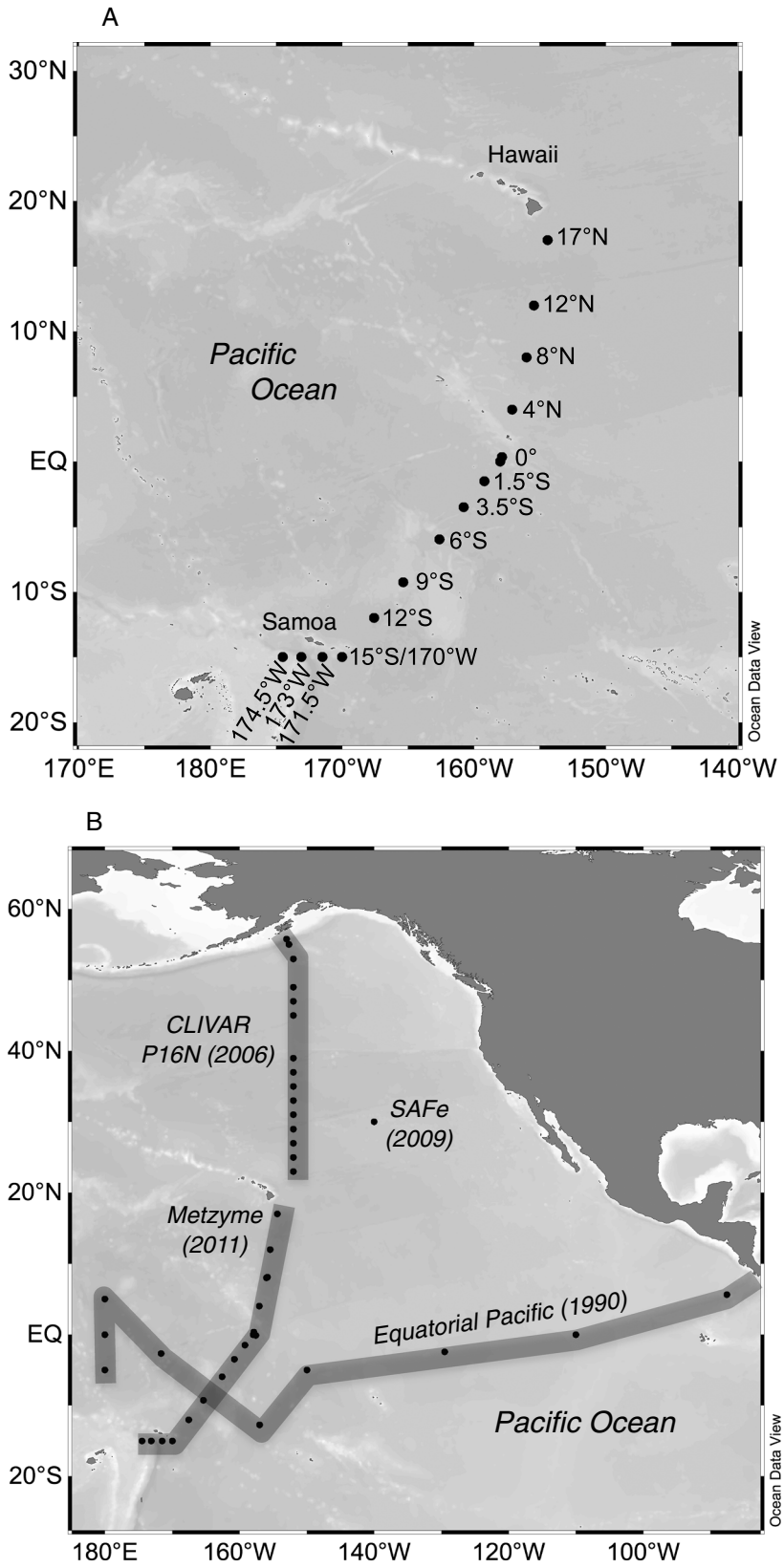

Figure 1. Map of Metzyme cruise stations. (a) The Metzyme cruise track. (b) The Metzyme cruise sampled water masses from which Hg species have been measured previously, including the Equatorial Pacific [*Mason and Fitzgerald*, 1990], the CLIVAR North Pacific P16N transect [*Sunderland et al.*, 2009], and at the SAFe station [*Hammerschmidt and Bowman*, 2012].

Table 1. Station Coordinates and Speciation Samples Collected at Each Station of Metzyme Cruise

Station	Latitude	Longitude	Samples
1	17°N	154°24′W	THg, Hg^0, DMHg, THg_{pump}, sediment traps
2	12°N	155°27′W	THg, Hg^0, DMHg, MMHg (0–1000 m)
3	8°N	156°W	THg, Hg^0, DMHg, MMHg, THg_{pump}, sediment traps
4	4°N	157°05′W	THg, Hg^0, DMHg, MMHg (0–1000 m)
5	0°	158°W	THg, Hg^0, DMHg, MMHg, THg_{pump}, sediment traps
6	3°30′S	160°46′W	THg, Hg^0, DMHg, MMHg, THg_{pump}
7	5°58′S	162°37′W	No Hg samples collected
8	9°15′S	165°22′W	THg, Hg^0, DMHg, MMHg, THg_{pump}
9	12°S	167°34′W	THg, Hg^0, DMHg, MMHg, THg_{pump}
10	15°S	170°W	THg, Hg^0, DMHg, MMHg
11	15°S	171°30′W	No Hg samples collected
12	15°S	173°06′W	THg, Hg^0, DMHg, MMHg
13	15°S	174°30′W	THg

limits of the previous North Pacific sampling locations and crossed through the Equatorial Pacific to the South Pacific. As a result, we are able to evaluate the spatial limits of the increases in total Hg observed in the North Pacific.

Here we present full dissolved and particulate speciation of Hg across significant biogeochemical gradients in the Central Tropical North and South Pacific, including deep waters at many stations. We use these measurements to evaluate the fluxes of mercury species from the surface to the intermediate waters and explore potential sources of methylated Hg. Our results reveal significant differences between the Hg inventories and cycling of the North Pacific compared to the Equatorial and South Pacific, excellent agreement with models of vertical fluxes for total Hg, corroborative evidence for insignificant vertical fluxes of MMHg, and insights into the rates of change in concentrations of total Hg in the subtropical North Pacific.

2. Materials and Methods

Dissolved and particulate mercury speciation was measured from a subset of stations (Table 1) occupied in the North and South Central Pacific Ocean between 3 and 24 October 2011 on board the R/V *Kilo Moana* (Figure 1). These stations were occupied as part of the "Metzyme" cruise, the goal of which was to explore the distribution and activity of micronutrients and metalloproteins in the ocean across a gradient of primary productivity and subsurface respiration. The northern section of the cruise sampled the oligotrophic waters of the North Pacific Subtropical Gyre before moving into the higher-productivity waters of the Equatorial Pacific. The lowest-productivity waters were sampled in the South Pacific. Water for dissolved Hg determination was sampled from eight stations roughly following a north to southwest transect beginning southeast of Hawaii at 17°N, 154°W and ending at 12°S, 168°W as well as two stations heading west along 15°S south of Samoa. Surface concentrations of dissolved Hg species were not measured. High-resolution measurements of atmospheric and aquatic gaseous Hg^0 from unfiltered surface water (7 m) along the Metzyme transect have recently been reported elsewhere [*Soerensen et al.*, 2014]. Suspended particles for Hg and MMHg determination were collected by deployment of large volume, in situ pumps at various depths at six stations spanning the north to southwest cruise transect. Sinking particles for THg and MMHg determination were collected in sediment traps deployed at three stations between 17°N and the equator.

Water for dissolved mercury speciation measurements was collected in acid-rinsed 8 L X-Niskin bottles attached to a dedicated epoxy-coated trace metal sampling rosette (SeaBird) and deployed on Amsteel line [*Noble et al.*, 2012]. Bottle sampling was triggered by a SeaBird Autofiring Module programmed to activate closure by pressure during up-casts. Niskin bottles were emptied on board in a positive pressure, HEPA-air-filtered water sampling bubble constructed from plastic sheeting. All dissolved species samples were collected under ultraclean N_2 pressure through 0.2 μm polyethersulfone filters (Supor), which have been observed to have little effect on dissolved Hg concentrations [*Bowman and Hammerschmidt*, 2011; *Lamborg et al.*, 2012].

Suspended particles were sampled from between 4 and 14 depths at six stations along the cruise track (Table 1) using in situ pumps (McLane Research Laboratories, Inc.). Sampling of suspended particles was biased toward stations north of the equator. Suspended particles were collected on combusted, acid-cleaned quartz microfiber filters (1 μm, Whatman QMA) after an in-line acid-cleaned polyester mesh prefilters (51 μm, Sefar Petex 07-51/33) to provide particles of two particulate size fractions. Subsamples of the large size fraction (>51 μm) were not available for Hg analysis; thus, we present particulate Hg data for the < 51 μm size fraction. The pumps were deployed for up to 3 h in order to pump ~1000 L of seawater through the filters. Filters that were installed and deployed but through which no water was pumped were processed as blanks.

Sinking particles were collected in acid-cleaned polycarbonate particle collection tubes with removable 250 mL low density polyethylene bottles as collection cups arranged in PVC frames at depths of 60 m, 150 m, and 500 m at stations 17°N, 8°N, and 0° using a surface-tethered system [*Lamborg et al*., 2008a]. Twelve tubes at each depth were deployed with a collection bottle at the bottom containing 250 mL of borate-buffered (pH = 8.2) seawater brine prepared from freezing filtered seawater and collecting the concentrated seawater as it melts. Above the brine, each tube was filled with filtered seawater (pH 8.2) [*Lamborg et al*., 2008a]. Three capped tubes were deployed in the trap array as process blanks. Upon recovery, the tubes were allowed to sit for 1 h to allow any particles in the tube to finish sinking. The collection bottles were then removed and the contents filtered on either preweighed polycarbonate membranes (1 μm, Nucleopore) or combusted quartz fiber filters (QMA). The membranes were used to determine mass and Hg species fluxes. The QMA filters were used for C and N flux determinations.

2.1. Hydrographic and Nutrient Data

Depth, salinity, temperature, and dissolved oxygen were measured by sensors on board a SeaBird Electronics SBE 19 deployed on the trace metal rosette. Nutrient (N + N, orthophosphate) samples were filled with filtered seawater during Niskin decanting, frozen on board, and measured by the laboratory of Joe Jennings at Oregon State University using standard methods [*Gordon et al*., 1994].

2.2. Total Mercury Determination

Filtered water for dissolved mercury speciation was sampled from the X-Niskin bottles into acid-cleaned 2 L Teflon bottles. Subsamples for total mercury (THg) were poured off into acid-cleaned 250 mL glass bottles (I-Chem) and oxidized with 0.2 mL of a bromine monochloride solution (~0.09 M in concentration trace metal grade HCl, JT Baker) for >1 h and prereduced with NH_2OH (0.2 mL 30% wt:vol). Samples were then reduced with $SnCl_2$, and total mercury concentrations were determined by dual Au-amalgamation cold vapor atomic fluorescence spectrometry with a Tekran 2600 against both gaseous Hg and aqueous Hg(II) standards (method recently summarized in *Lamborg et al*. [2012]). Reagents were prepared according to U.S. EPA Method 1631 [*U.S. Environmental Protection Agency* (*EPA*), 2002].

2.3. Gaseous Mercury Determination

Gaseous elemental (Hg^0) and dimethylmercury (DMHg) were purged directly from the remaining seawater in the 2 L Teflon bottles using a multiport cap (Omnifit Q-series; Danbury, CT) outfitted with a purge line with a fine pore frit that extended to the bottom of the bottle. Hg^0 and DMHg were purged from the seawater sample using ultrapure N_2 gas (0.5 L min^{-1}) for 1 h. The gaseous species were separated and preconcentrated onto a gold-coated sand trap attached downstream of a Tenax trap in outlet of the purge cap [*Lamborg et al*., 2008a]. After purging, traps were dried with Ar gas flow for 2 min. Hg^0 was determined using a Tekran 2600, while DMHg was determined using a Tekran 2500 following isothermal GC separation and pyrolysis to Hg^0. Both analytical systems were calibrated with Hg^0 standard addition.

2.4. Methylmercury Determination

Following purging of gaseous mercury species, ~200mL subsamples for MMHg determination were poured from the 2 L Teflon bottles into acid-cleaned 250 mL amber glass bottles (I-Chem) and acidified to 0.5% with concentrated H_2SO_4 (trace metal grade, Fisher Scientific). Samples were stored at 4°C and analyzed at the Woods Hole Oceanographic Institution (WHOI) using ascorbic acid-assisted direct ethylation [*Munson et al*., 2014]. Samples were buffered with either 2 M acetic acid or 1 M citric acid buffer (pH 5) and neutralized with KOH (45%) to pH 5. The addition of ascorbic acid (0.17% final vol/vol) allowed for enhanced MMHg

determination from seawater after direct derivatization with sodium tetraethylborate (1%, in 2% KOH) and gave detection limits around 5 fM. Reagents were prepared according to U.S. EPA Method 1630 [*EPA*, 1998].

Sample bottles were fitted with Teflon backed silicon septa caps (I-Chem) and run on a Tekran 2700 Automated Methylmercury Analyzer equipped with a custom autosampler tray. MMHg concentrations were determined versus linear standard curves prepared daily with MMHg standard solution (Alfa Aesar).

2.5. Particulate Mercury

Suspended and sinking particulate THg and MMHg were determined from weighed filter portions. For suspended particles, 2.5 cm punches from 14.2 cm filters were analyzed. For sinking particles, 25 mm filters were quartered with ceramic scissors for analysis. Weights were determined by zeroing balance between triplicate samples using antistatic gun (Zerostat 3, Milty). All recorded filter weights were greater than the uncertainty of weighing. MMHg and THg in suspended and sinking particles were determined by digesting weighed filter portions in HNO_3 (2N, trace metal grade, Fisher) for 4 h at 60°C with intermittent sonication. Digests were either oxidized with BrCl and processed as described above for THg determination or processed as described above for MMHg determination with direct ethylation. Suspended particulate Hg species are presented as concentrations representing the measured THg or MMHg collected on filters from known volumes of filtered seawater. Total filter mass was not determined.

2.6. Particulate Carbon and Nitrogen Analysis

Particulate carbon and nitrogen determinations were made on both sinking and suspended matter through high-temperature combustion analysis (Flash EA1112) of quartz fiber filter subsamples in WHOI's Nutrient Analytical Facility. For these samples, no attempt was made to distinguish between organic and inorganic particulate carbon.

3. Results

3.1. Parameters

Salinity profiles of the cruise transect display the transition between North Pacific Intermediate Waters at 17°N and more uniform salinity in surface waters between 8°N and 12°N. At these latitudes, the convergence of the North Equatorial Current and the North Equatorial Counter Current appears to the segregate shallower waters (<400 m) of the North Pacific the Equatorial Pacific (S ~34.5) from one another (Figure 2b).

Dissolved O_2 concentrations reveal that the transition between the North and Equatorial Pacific observed at these latitudes is the western extension of the strong oxygen minimum zone from the eastern tropical North Pacific, with < 2 μmol/kg O_2 measured between 200 and 900 m at 12°N (Figure 2e). The extent to which these low O_2 concentrations at 12°N may influence metabolic function was estimated by calculating the parameter N* [*Gruber and Sarmiento*, 1997; *Deutsch et al*., 2001] from measured nitrate and phosphate concentrations according to the following equation:

$$N^* = [NO_3^-] - ([PO_4^{3-}]*16) + 2.9 \text{ mmol m}^{-3}$$

N* will exhibit positive values if nitrogen fixation is a significant source of fixed nitrogen to a water mass, while negative values suggest deficits of fixed nitrogen due to denitrification. In subsurface waters, 150–400 m, at 12°N values of N* range between −6.7 and −8.1 (Figure 3), suggesting dentrification at these depths depletes concentrations of NO_3^- relative to Redfield stoichiometry [*Gruber and Sarmiento*, 1997].

Shoaling of nutrients and the seasonal thermocline is observed at the edge of the North Pacific Subtropical Gyre. Upwelling of dissolved nutrients is apparent in the upper 150 m at 0°, where concentrations of $PO_4 > 0.6$ μmol/L and $NO_3 > 6$ μmol/L persist. South of the equator, high-salinity waters are observed above a seasonal thermocline that extends deeper in the water column to the south.

Apparent oxygen utilization ($[O_2]_{sat} - [O_2]_{meas}$) (*Garcia and Gordon* [1992] as modified by *Sarmiento and Gruber* [2006]) values were also used to estimate the extent of cumulative organic matter remineralization (Figure 2f). High values of AOU are largely limited to the intermediate waters north of the equator and indicate the higher productivity of these waters relative to those of the South Pacific (Figure 2f).

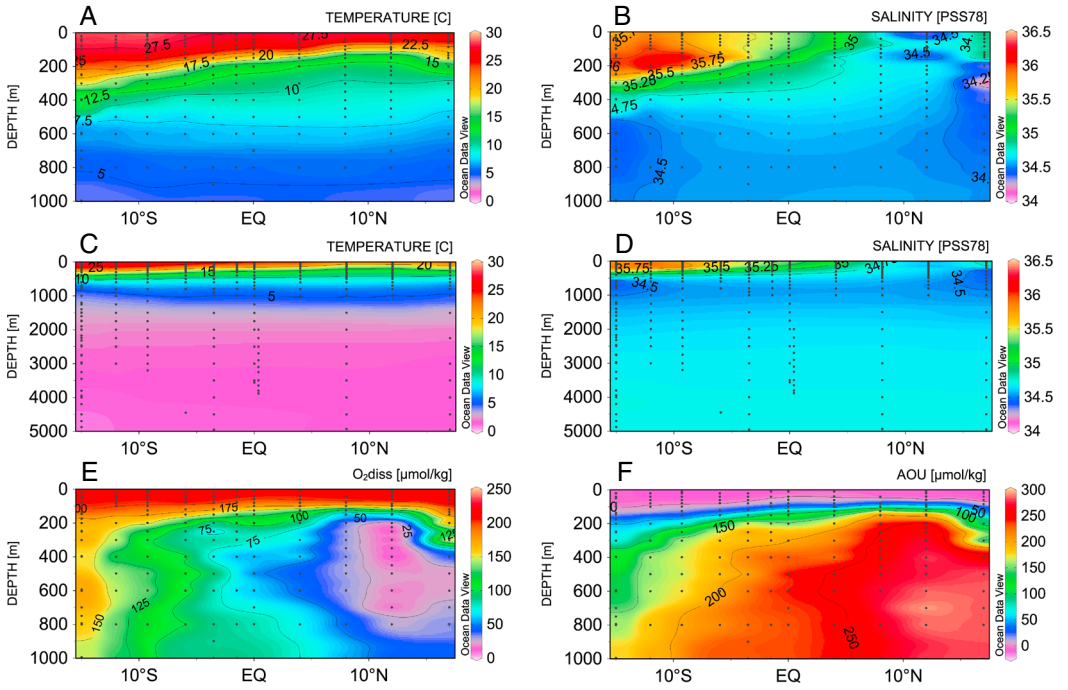

Figure 2. Hydrographic characteristics of the north to south transect of the Metzyme cruise. (a) Temperature and (b) salinity in the upper 1000 m of water column. (c) Temperature and (d) salinity within the full water column. (e) Dissolved oxygen and (f) AOU in the upper 1000 m. Values of AOU are closely related to dissolved oxygen concentrations, with highest oxygen utilization centered at Station 2 (12°N) and extends to below the North Pacific Subtropical Gyre at Station 1 (17°N) and beneath the sharp oxycline at Station 3 (8°N) (Figure 2f). South of the equator, gradients of both dissolved oxygen concentrations and AOU are weak throughout intermediate waters.

3.2. Dissolved Mercury Speciation

3.2.1. Total Mercury

Surface concentrations of THg are low, $<$ 0.5 pM, for all stations (Figures 4a and 5a). These low concentrations extend through the mixed layer, ~75 m north of the equator and to depths ~125 m south of the equator. Below the mixed layer, THg concentrations approach ~1 pM reaching a maximum of ~1.5–2.0 pM in intermediate waters ($<$1000 m in depth) in the North Pacific Intermediate water (17°N) and Equatorial waters (4–8°N). However, these regions of THg are separated from one another by the low dissolved O_2 region at 12°N (Figure 2e). South of the equator, dissolved THg concentrations decrease to 0.8 pM in intermediate waters.

Elevated concentrations of THg (1.5–2 pM) are observed in deep waters (below 2000 m) at the northern end of the cruise transect, at 17°N (Figure 4b), and decrease (1.25–1.5 pM) to the south in deep waters south of the equator at 5°S (Figure 5b). This gradient in THg concentrations results from the very old Pacific Bottom Water moving south until it mixes with and is replaced at depth ($>$4500) by Lower Circumpolar Deep Water, which is considerably younger [*Talley et al.*, 2011]. As a result average THg concentrations (~1 pM) in deep water south of 5°S fall within the range of those measured in the Antarctic Bottom Water in the Southern Ocean (0.98–1.99 pM) [*Cossa et al.*, 2011].

3.3. Elemental Mercury

Filtered Hg^0 shallow samples (10 m) were collected from two stations, 12°N and 0°, and were lower than unfiltered surface samples (7 m) [*Soerensen et al.*, 2014] by 45% and 5%, respectively. Deeper filtered Hg^0 samples (20 m) from five stations were also lower than unfiltered surface samples collected by Soerensen and colleagues (average 2%; range 1% to 92%) [*Soerensen et al.*, 2014].

Concentrations of Hg^0, like those of THg, are low in the mixed layer with highest concentrations at 17°N and 12°N, where Hg^0 approaches 0.1 pM (Figure 4). Concentrations of Hg^0 generally increase below the mixed layer, reaching maximum concentrations in the upper water column immediately below the thermocline.

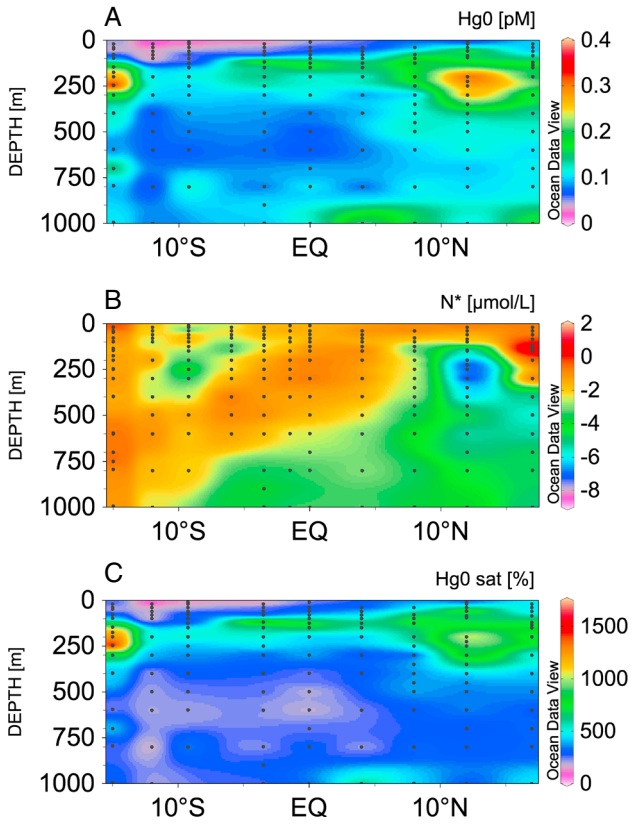

Figure 3. Net mercury reduction coincident with denitrification at the southern base of the North Pacific Subtropical Gyre. Upper 1000 m of transect from 17°N to 15°S showing (a) measured Hg^0 concentrations, (b) N* calculated from measured [PO_4^{3-}] and [NO_3^-], and (c) percent saturation of Hg^0. The maximum in Hg^0 concentrations between 200 and 400 m at 12°N correspond with indications of denitrification from N*. In contrast to maximum at 12°N, maximum at 15°S does not correspond to denitrification.

Two features are noted within this region immediately below the thermocline in the upper ocean profiles of Hg^0. At 12°N, a large Hg^0 maximum of 0.2–0.4 pM is focused at depths between 200 and 400 m (Figure 3). This station falls within the intertropical convergence zone (ITCZ) (5–14°N), where surface Hg^0 concentrations are elevated, more than twice that of other regions measured along the Metzyme transect [*Soerensen et al.*, 2014]. A second maximum of 0.2–0.35 pM Hg^0 was measured between 150 and 350 m at 15°S, 170°W (Figure 3).

Minimum concentrations of Hg^0 are generally observed immediately beneath the maximum concentrations at the base of the mixed layer, resulting in low concentrations in intermediate waters (Figures 3). In the South Pacific, this minimum is broad and extends to depths of 1000 m. In the North Pacific, this minimum is narrow and concentrations quickly increase from ~0.1 pM to 0.2 pM. In addition, at several depths within the region of the deep North Pacific where elevated THg was measured, Hg^0 concentrations increase to 0.2–0.3 pM (Figure 4b).

As is typical of marine waters [*Kim and Fitzgerald*, 1986; *Mason and Fitzgerald*, 1993; *Mason et al.*, 1998; *Horvat et al.*, 2003; *Lamborg et al.*, 2008b], the Central Pacific is supersaturated with respect to Hg^0 (Figure 3c). Furthermore, the distribution of percent Hg^0 saturation matches the concentration gradients (Figures 3a and 3c). At 12°N and 15°S, 170°W, percent Hg^0 saturation is upward of 1000% within the subsurface Hg^0 maxima (Figure 3c).

3.4. Monomethylmercury

Concentrations of MMHg approach detection limits (~5 fM) in much of the surface ocean, with the exception of the equator, where concentrations vary between 15 and 70 fM in the upper 200 m (Figure 4a). In the upper 1000 m of the ocean, MMHg appears to be distributed slightly asymmetrically around the equator, with higher MMHg concentrations north of the equator relative to south (Figures 4a and 5a). The highest concentrations of MMHg observed along the cruise transect, 150–165 fM, are seen at the depths of the oxygen minimum at the equatorial station. MMHg concentrations in the deep equatorial region are also elevated with respect to adjacent stations. MMHg concentrations increase from ~50 fM to 85–155 fM between 2000 and 3500 m at the equator (Figure 4b). At 12°N, the low surface concentrations of MMHg extend to 400 m in the region where Hg^0 concentrations are elevated (Figure 4a). No MMHg samples were collected from the 17°N station. We estimate that total methylated Hg (MeHg = [MMHg] + [DMHg]) values in the North Pacific Intermediate Water at 17°N are similar in magnitude to those measured previously in the North Pacific (Table 2), which averaged 95 ± 114 fM above 150 m and 260 ± 114 fM between 150 and 1000 m [*Sunderland et al.*, 2009].

3.5. Dimethylmercury

Concentrations of DMHg are generally higher than those of MMHg. In contrast to MMHg, DMHg in the surface ocean (>20 m) was often above our detection limit, ~20 fM (Figures 4a and 5a). Concentrations of DMHg,

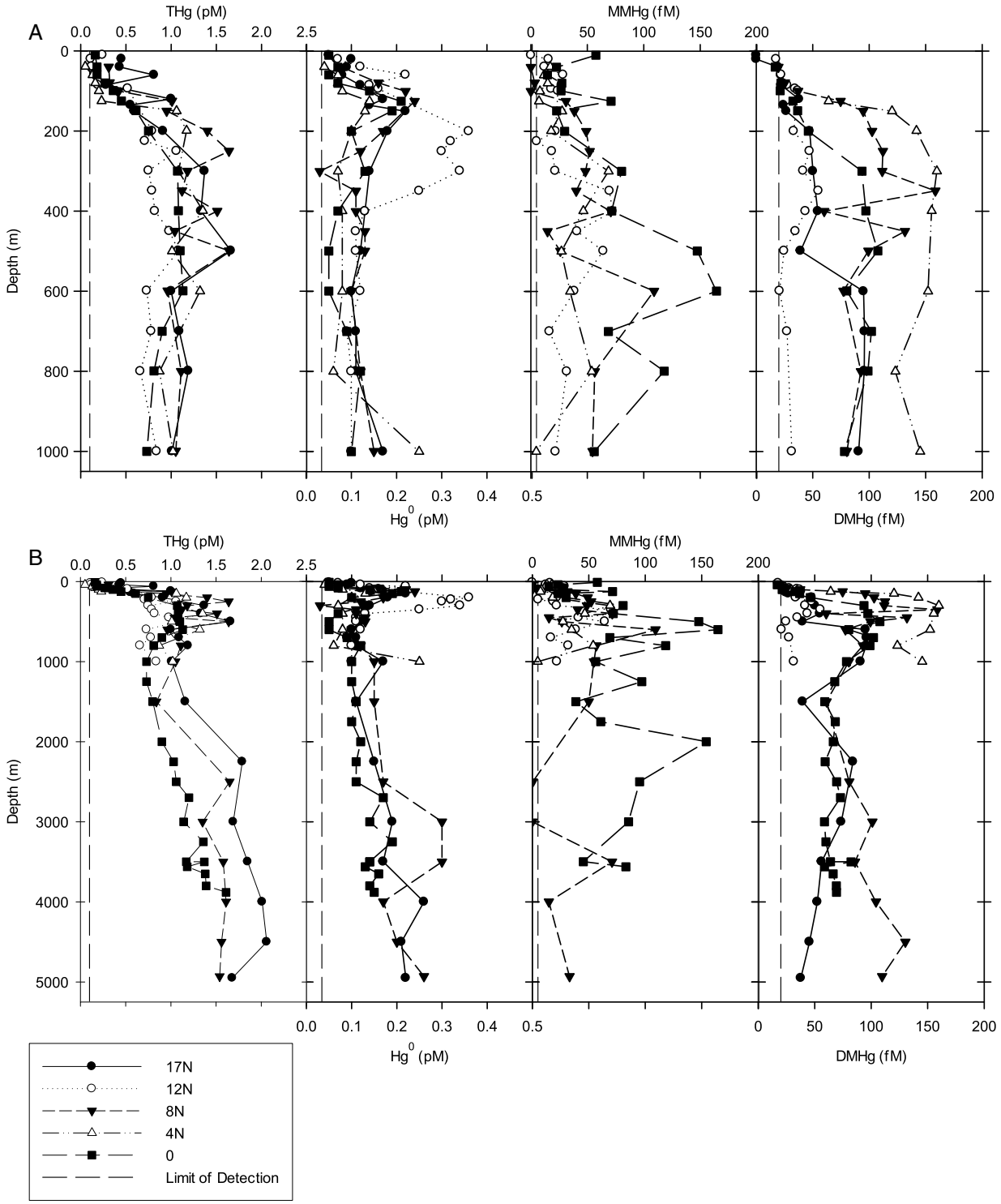

Figure 4. (a) Upper 1000 m and (b) full water column concentration profiles of dissolved Hg species from Metzyme stations between 17°N and the equator. THg and Hg^0 concentrations are shown in pM. MMHg and DMHg concentrations are shown in fM. Concentrations of all dissolved species are low in surface waters and enhanced in intermediate waters. Limits of detection for each species are represented by vertical dashed lines.

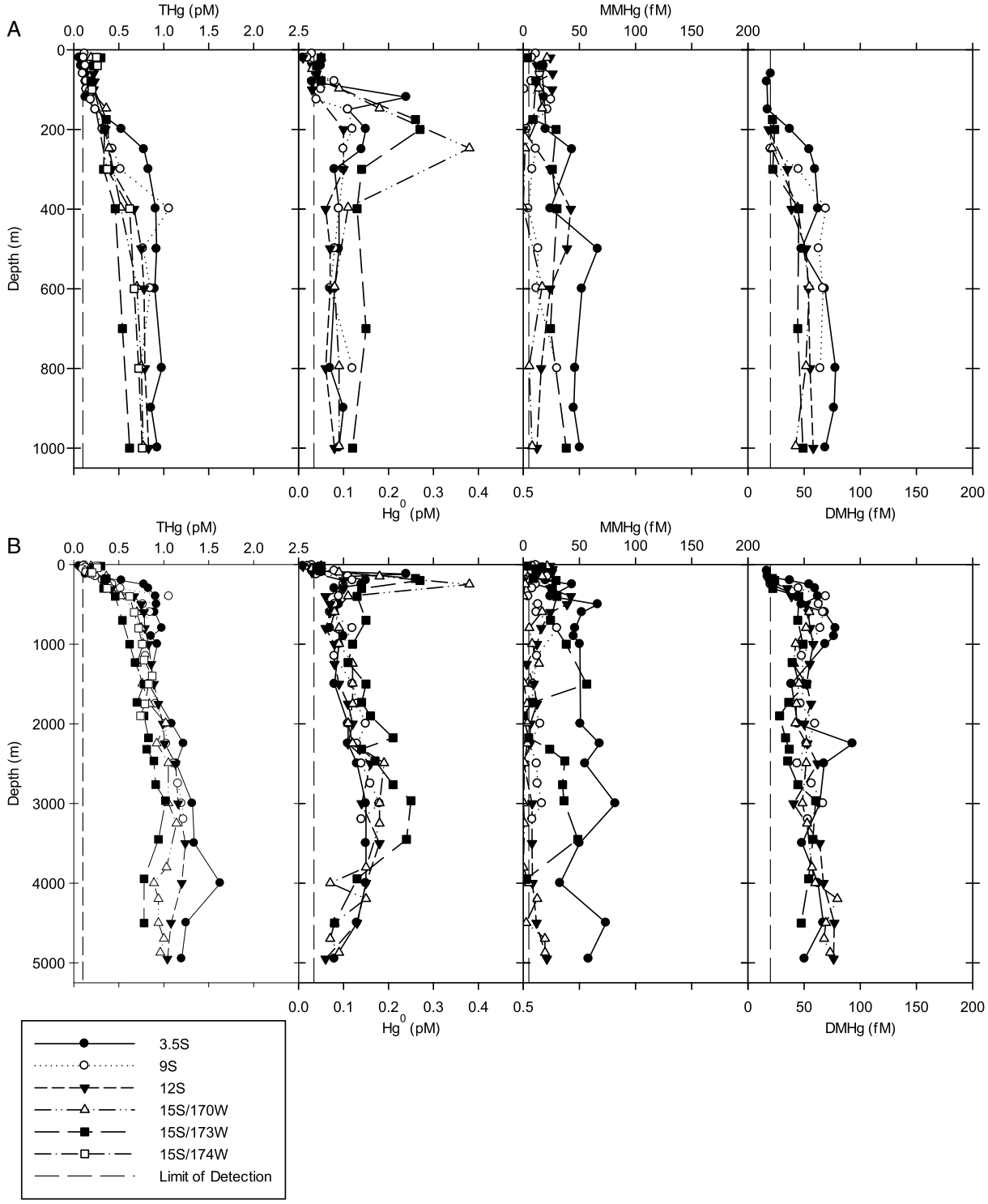

Figure 5. (a) Upper 1000 m and (b) full water column concentration profiles of dissolved Hg species from Metzyme stations located south of the equator. THg and Hg^0 concentrations are shown in pM. DMHg and MMHg concentrations are shown in fM. Limits of detection for each species are indicated by vertical dashed lines.

like MMHg, reach their maximum, 120–160 fM, at depths with low oxygen concentrations. However, it is important to note that the highest DMHg concentrations are found at depths with intermediate dissolved O_2 concentrations (~60 µmol/kg) rather than minimum dissolved O_2 concentrations, which we would expect if methylation was primarily controlled by organic matter remineralization. Like MMHg, DMHg is distributed

Table 2. Average Concentrations of Hg Species From the Pacific Ocean[a]

Basin	Depth	THg (pM)	Hg^0 (pM)	DMHg (fM)	MMHg (fM)	MeHg (fM)	%MeHg
			This Study				
17°N–8°N	Within thermocline	0.54 ± 0.36	0.14 ± 0.06	35 ± 21	17 ± 14	66 ± 39	20 ± 11
	Intermediate	1.06 ± 0.29	0.15 ± 0.08	70 ± 36	43 ± 24	115 ± 47	11 ± 4
	Deep	1.70 ± 0.20	0.22 ± 0.05	80 ± 28	24 ± 30	125 ± 33	8 ± 2
4°N–3.5°S	Thermocline	0.29 ± 0.26	0.10 ± 0.06	38 ± 30	24 ± 17	73 ± 34	17 ± 7
	Intermediate	0.96 ± 0.17	0.10 ± 0.04	92 ± 36	62 ± 39	160 ± 49	16 ± 4
	Deep	1.25 ± 0.18	0.13 ± 0.03	65 ± 11	71 ± 30	136 ± 34	12 ± 5
6°S–15°S	Thermocline	0.29 ± 0.14	0.09 ± 0.08	31 ± 11	15 ± 10	50 ± 19	11 ± 4
	Intermediate	0.77 ± 0.10	0.10 ± 0.03	53 ± 8	17 ± 14	70 ± 17	9 ± 3
	Deep	0.98 ± 0.14	0.14 ± 0.04	54 ± 13	12 ± 12	67 ± 17	7 ± 2
			Previous Studies				
North Pacific	Above thermocline[b]	0.6 ± 0.30		5–20	20–100	170	
	Below 1500 m[b]	1.20 ± 0.30				120	
	<150 m[c]	0.99 ± 0.32 (0.5–1.94)				95 ± 114 (59–470)	10 ± 5 (2–24)
	>150 m[c]	1.35 ± 0.37 (0.65–2.39)				260 ± 114 (59–470)	19 ± 6 (5–29)
	Above thermocline[d]	0.3–1.0					
	Below thermocline[d]	1.0–1.5		13 ± 1	24 ± 4		
Equatorial Pacific	0–1000 m[e]	1.70 ± 1.22 (0.40–6.90)	0.25 ± 0.16 (0.02–0.69)	170 ± 170 (10–670)	113 ± 108 (45–580)	180 ± 220 (0–920)	

[a]To facilitate comparison with other studies, mean concentrations (±1 standard deviation) for dissolved Hg species grouped into the North Pacific (17°N–8°N), Equatorial Pacific (4°N–3°S), and South Pacific (6°S–15°S). Previously published Pacific data are included as well. Because no MMHg samples were collected at 17°N, MMHg, MeHg, and %MeHg, averages are shown for 12°N–8°N.
[b]*Laurier et al.* [2004].
[c]*Sunderland et al.* [2009].
[d]*Hammerschmidt and Bowman* [2012].
[e]*Mason and Fitzgerald* [1993].

asymmetrically across the equator but with the maximum concentrations measured at 4°N (Figure 4a). Beneath the mixed layer, DMHg concentrations average 75 fM with slightly lower concentrations south of the equator (Figures 4 and 5). In the deep ocean, elevated DMHg concentrations of 100 fM were measured at several depths within waters with elevated THg concentrations, most notably at 8°N (Figure 4b).

Unlike THg, MeHg concentrations in the deep waters south of 5°S (0.067 ± 0.017 pM, Table 2) were markedly lower than those measured in Antarctic Bottom Water (AABW) (0.52 ± 0.11 pM) [*Cossa et al.*, 2011]. The differences in concentrations indicate demethylation of MeHg during the transport of AABW toward the deep waters of the South and Equatorial Pacific. Assuming 600 years as the time for transport of AABW from the Southern Ocean to the measured waters of 6–15°S in the South Pacific [*Khatiwala et al.*, 2012], we estimate a residence time of MeHg in the South Pacific with respect to input from AABW as 292 years compared to a residence time of 436 years for THg. This reflects the likely demethylation of MeHg and conversion into the inorganic Hg pool, as is indicated by the lower MeHg concentrations as well as decreases in the percentage of THg as MeHg from ~22% in AABW [*Cossa et al.*, 2011] to 7% in the South Pacific (Table 2).

3.6. Suspended Particulate Mercury Speciation

Suspended particles collected from in situ pumps have low concentrations of both THg (THg_{susp}) and MMHg ($MMHg_{susp}$) relative to their dissolved concentrations. THg_{susp} ranged from 0.01 to 0.05 pM from all stations and averaged 5.3% (range: 1.0–27.4%) of dissolved THg concentrations (Figure 6). $MMHg_{susp}$ ranged from 0.1 to 3.1 fM and averaged 3.7% (range: 0.2–12.8%) of dissolved MMHg concentrations (Figure 6). Previous measurements of Hg species in the Pacific have not distinguished between dissolved and particulate species [*Mason and Fitzgerald*, 1993; *Laurier et al.*, 2004; *Sunderland et al.*, 2009]. However, the generally low percentages of THg_{susp} and $MMHg_{susp}$ allow us to compare our measured values to those previously determined in the Pacific.

Concentrations of THg_{susp} decrease slightly from the northern to southern ends of the cruise transect. THg_{susp} concentrations average 0.03 ± 0.001 pM at 17°N ($n = 8$), 8°N ($n = 14$), 0° ($n = 13$). South of the equator, the concentration falls to 0.02 ± 0.002 pM at 3°S ($n = 4$), 9°S ($n = 4$), and 12°S ($n = 3$). There is no

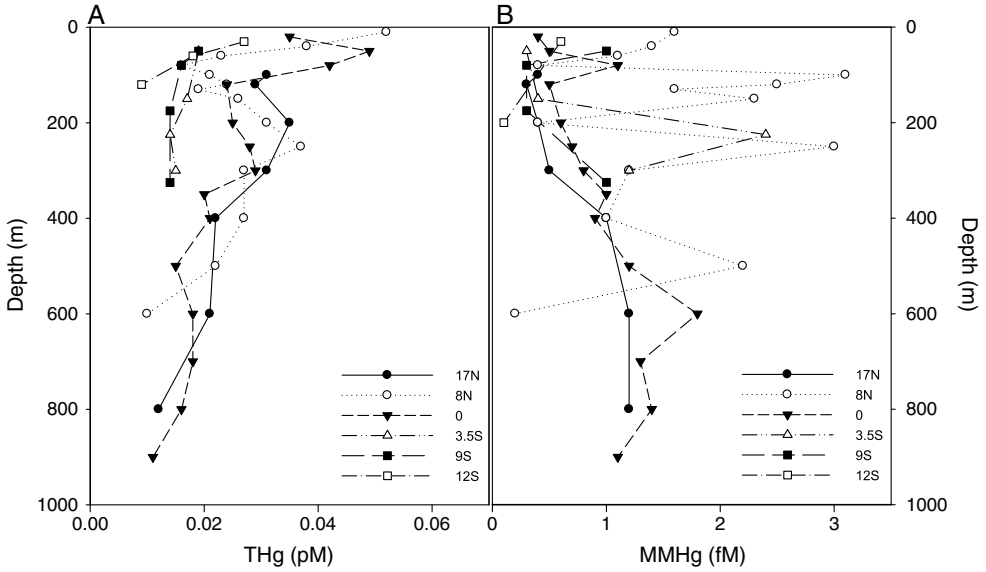

Figure 6. Concentrations of suspended particulate (a) THg (pM) and (b) MMHg (fM) collected by in situ pump in upper and intermediate waters.

significant change in the percentage of THg_{susp} relative to dissolved THg with latitude. Average $MMHg_{susp}$ concentrations, with the exception of 17°N (0.7 fM, $n = 8$), roughly decrease from 8°N (1.6 fM, $n = 14$) to 12°S (0.4 fM, $n = 2$).

Although the concentrations of THg_{susp} and $MMHg_{susp}$ are negligible compared to their respective dissolved concentrations, the depth distributions of each suggest differences in the cycling of different Hg species. THg_{susp} concentrations are generally highest within the upper 50 m of the water column, consistent with higher particle abundance in surface waters (Figure 6). In contrast, $MMHg_{susp}$ concentrations are highest within 100 m of the depth of minimum dissolved O_2 concentration at each station measured (Figure 6). The only exception to these trends are at 17°, where THg_{susp} could not be measured within the upper 50 m and 12°S, where $MMHg_{susp}$ was not measured at 400 m, where the dissolved O_2 concentration was lowest.

3.7. Sinking Particulate Mercury Speciation

Total mass fluxes were below detections limits (20–23 mg/m^2/d) at all depths at 17°N and at 500 m at 8°N (Table 3). Overall, mass fluxes decrease from the equatorial station northward, with surface fluxes at 0° twice that of 8°N (Table 3).

Like total mass fluxes, sinking particulate Hg fluxes attenuate with depth at each station, approaching 31.3 ± 12.0 pmol/m^2/d at 500 m for all three stations (Table 4). Fluxes from the mixed layer were highest (156.6 pmol/m^2/d) at the equator and lowest (36.7 pmol/m^2/d) at 17°N. Assuming 80% of wet and dry Hg

Table 3. Particulate Carbon Flux Calculations From Three Particle Trap Deployments in the North and Equatorial Pacific Ocean[a]

	Total Flux (mg/m^2/d)[b]			C_{part} (μmol/m^2/d)			$(THg/C)_{part}$		
Depth	17°N	8°N	0°	17°N	8°N	0°	17°N	8°N	0°
60 m	21 ± 3[b]	108 ± 66	232 ± 75	1711 ± 271	6925 ± 1993	10006 ± 1968	0.02	0.01	0.02
150 m	13 ± 2[b]	43 ± 26	82 ± 10	467 ± 253	961 ± 94	1946 ± 341	0.06	0.04	0.06
500 m	11 ± 9[b]	6 ± 0[b]	45 ± 13	347 ± 48	418 ± 204	604 ± 108	0.05	0.08	0.07

[a]Flux values (±1 standard deviation) from triplicate measurements of carbon collected during 24 h sediment trap deployments. Ratios of particulate THg (Table 4) and C are also shown.

[b]Results are below detection limit calculated as 3 times the standard deviation of blank filters 60 m: 23 (mg/m^2/d); 150 m: 21 (mg/m^2/d); 500 m: 20 (mg/m^2/d).

Table 4. Particulate THg and MMHg Data From Three Pacific Ocean Stations[a]

	THg (pmol/m^2/d)			MMHg (pmol/m^2/d)[b]		
Model/Measure	17°N	8°N	0°	17°N	8°N	0°
			Atmospheric Deposition (wet + dry)			
MITgcm[c]	136	213	136			
			Ocean Sinking Particulate Flux			
MITgcm	4.5	6.7	27.5			
Metzyme 60 m	37 ± 37	55 ± 32	157 ± 58	0 ± 0.82	1.63 ± 3.08	1.48 ± 2.47
Metzyme 150 m	30 ± 34	38 ± 25	123 ± 23	0.14 ± 0.80	1.02 ± 0.16	0.41 ± 0.93
Metzyme 500 m	18 ± 18	34 ± 35	42 ± 19	0.51 ± 0.44	0.01 ± 0.49	0.12 ± 0.32

[a]Flux values (±1 standard deviation) from triplicate measurements of THg and MMHg collected during 72 h sediment trap deployments. MITgcm model fluxes of THg deposition and sinking from the mixed layer [*Soerensen et al*., 2014] are shown for comparison.
[b]Detection limit is 1.52 pmol/m^2/d (from 3 times the standard deviation of blanks).
[c]Total deposition shown.

deposition is rapidly evaded in the surface ocean [*Mason and Sheu*, 2002; *Strode et al*., 2007; *Soerensen et al*., 2010], measured particulate fluxes at all stations exceed the remaining deposited Hg, modeled by MITgcm [*Soerensen et al*., 2014] (Table 4). The observed fluxes therefore require additional inputs of Hg to Tropical Pacific waters, most notably at the equator, where upwelling supplies dissolved THg for the subsequent sinking flux.

A simple one-dimensional model of the equatorial THg demonstrates the influence of upwelling on the measured sinking flux. Assuming an upwelling velocity of 2.5 m/d [*Bryden and Brady*, 1985] transporting water from depths ~100 m from adjacent stations (0.2 pM at 4°N, 0.13 pM at 3°S), into the mixed layer, the upwelling flux of dissolved THg is 400 pmol/m^2/d. Given the modeled MITgcm atmospheric input that persists in the water column (i.e., is not rapidly evaded) at 0° (Table 4) compared to the measured sinking flux of 156.6 pmol/m^2/d at 60 m, upwelling can more than account for the THg that is exported from the mixed layer to intermediate waters by particle remineralization. Indeed, using these values, inputs from upwelling and deposition exceed sinks from evasion and particle scavenging by about 270 pmole/m^2/d, implying that the equatorial region exports THg laterally through advection. Using the inventory of dissolved THg in the upper 60 m at 0° from measured values (0.16–0.18 pM), the resulting residence time of dissolved THg with respect to the upwelling and deposition supply is 24 days. The MITgcm treatment of all the fluxes in and out of the surface ocean comes to much the same conclusion [*Soerensen et al*., 2014]. The modeled sinking fluxes at all stations, as well as the upwelling flux at the equator, are substantially lower than our measured fluxes (~5 times lower). However, the modeled and measured fluxes do scale with each other well ($r^2 = 0.99$), which encourages the view that the model captures the essential dynamics of Hg cycling in the region well.

Measured values of sinking particulate MMHg fluxes throughout the upper water column were small, between 0 and 1.63 pmol/m^2/d. However, the majority of these values were not above the relatively high detection limit of 1.52 pmol/m^2/d. Assuming the values are accurate, however, sinking fluxes of MMHg represent between 0 and 3.0% of THg sinking fluxes.

The upwelling flux of dissolved MMHg (8.13 fM at 4°N, 18.75 at 3°S) to the mixed layer at the equatorial station is 33.6 pmol/m^2/d, which is higher than the 1.63 pmol/m^2/d measured as the sinking flux from 60 m (Table 4). The residence time with respect to upwelling for dissolved MMHg above 60 m at the equator is 51 days (assuming the atmospheric deposition flux of MMHg is minimal) [*Lamborg et al*., 1999]. The ratio of MMHg: THg is consistent both within and below the mixed layer. Therefore, the longer residence time of MMHg compared to THg reflects differences in the sources and sinks of the two species to the mixed layer, most likely due to evasion of Hg^0 and/or in situ production of MMHg in these waters. Methylation would have to account for an input of 71 pmol/m^2/d to equate the residence time with respect to upwelling of MMHg with that of THg. The average methylation rate measured in the surface mixed layer of Mediterranean Sea and Canadian Arctic Archipelago seawater [*Monperrus et al*., 2007; *Lehnherr et al*., 2011] would yield methylation inputs between 2 and 390 pmol/m^2/d, which could be sufficient to account for the addition source of MMHg in the surface mixed layer.

Table 5. Average Ratios of Dissolved MMHg to DMHg Along the Metzyme Cruise Track[a]

Station	MMHg:DMHg	Max Depth (m)
12°N	1.15 ± 0.76 (0.38–3.21)	500
8°N	0.46 ± 0.37 (0.04–1.36)	599
4°N	0.24 ± 0.15 (0.03–0.45)	800
0°	1.19 ± 0.53 (0.57–2.37)	125
3°S	0.86 ± 0.31 (0.41–1.37)	500
9°S	0.24 ± 0.14 (0.07–0.57)	250
12°S	0.29 ± 0.28 (0.08–1.06)	400
15°S/170°W	0.16 ± 0.09 (0.07–0.35)	595
15°S/173°W	0.64 ± 0.42 (0.10–1.46)	200
All Stations	0.58 ± 0.54 (0.03–3.21)	

[a]Ranges shown in parentheses. Depth of maximum MMHg:DMHg for each station also shown.

Carbon flux data collected from sediment traps at 17°N, 8°N, and 0° reflect the differences in productivity along the northern section of the cruise transect. At 60 m, the carbon flux at 17°N (1711 ± 271 μmol/m^2/d) is less than 20% of that at 0° (10006 ± 1968 μmol/m^2/d) (Table 3). Nitrogen fluxes showed an identical pattern and C:N ratios of 7.7 ± 2.6 (range: 5.3–13.9; $n = 12$), which is slightly enriched in C relative to Redfield stoichiometry between 6.2 and 6.6.

In comparison with C (or N), the Hg flux attenuation is less pronounced. The ratio of THg:C in the sediment trap material generally increases with depth between 60 m to 500 m (Table 3). This increase reflects a preferential removal of Hg from the surface ocean relative to carbon export in Central Pacific waters.

3.8. Relative Concentrations of Monomethylmercury and Dimethylmercury

Increases in the molar ratios of MMHg:DMHg in low-O_2 depths at the SAFe station (30°N, 140°W) in the North Pacific have been interpreted as deviations from steady state exchange of methyl groups between Hg species [*Hammerschmidt and Bowman*, 2012]. Generally, at northern stations (between 12°N and 0°), MMHg concentrations are similar to those of DMHg throughout the water column, with the range of MMHg:DMHg values between 0.03 and 2.4 for all stations (Table 5). The only exception to this range is a local maximum of 3.2 at 500 m near the base of the Hg^0 maximum at 12°N where DMHg is more severely depleted relative to MMHg. South of 3°S, MMHg concentrations decrease relative to those of DMHg and MMHg:DMHg values fall below 1.5 for all depths. At Station 15°S, 173°W, MMHg concentrations are once again comparable to those of DMHg.

4. Discussion

4.1. Controlling Inorganic Mercury Speciation

The low surface water THg concentrations are consistent with removal by reduction of Hg(II) to Hg^0 and subsequent evasion as well as particle export [*Soerensen et al.*, 2014]. The export of particulate THg results in increases of THg concentrations in intermediate waters that correspond to regions of net organic matter remineralization. The general decrease from the North Pacific to the South Pacific reflects the fivefold decrease in modeled fluxes of particulate THg in the South Pacific relative to the productive equatorial region [*Soerensen et al.*, 2014].

The elevated concentrations of THg observed at depth are likely the result of differences in productivity and the extent of remineralization between deep waters of the North and South Pacific basins. Salinity values suggest that the observed attenuation of the elevated THg seen in depth profiles is likely the increasing influence of Antarctic Bottom Water (AABW, S 34.65–34.75) south of North Pacific Bottom Water. The concentration of THg in these higher-salinity waters (<1.3 pM from 9°S, 4500–5000 m southward) is within the range (1.35 ± 0.39 pM) measured recently in AABW [*Cossa et al.*, 2011].

The maximum of Hg^0 is observed at 12°N where dissolved O_2 concentrations are lowest, < 2 μm/kg. Comparing Hg^0 concentrations to patterns of N*, the maximum in Hg^0 at 12°N between 100 and 400 m corresponds to a local deficit in [NO_3^-] relative to Redfield stoichiometry. At 12°N, values of N* vary from −6 to −8 mmol/m^3 (Figure 3), which are consistent with denitrification occurring at these depths. No direct link between marine denitrification and Hg reduction has been noted previously in the literature, although microbial mediated Hg reduction has been observed in marine systems [*Mason et al.*, 1995; *Rolfhus and Fitzgerald*, 2004; *Poulain et al.*, 2007]. Denitrification has been implicated as a pathway of Hg(II) reduction by *mer* operon-mediated reduction in bacteria studied in vitro [*Schaefer et al.*, 2002;

Kritee et al., 2007]. Therefore, it is plausible that the observed peak in Hg^0 at 12°N is induced by the strong denitrification at this location. However, calculations of N* in waters along the transect show no additional regions where denitrification occurs to the extent that it does at 12°N. Therefore, the potential for denitrification to influence Hg speciation on basin scales will have to be tested using future measurements of Hg^0 in regions of denitrification.

Recently, *Soerensen et al*. [2014] attributed elevated surface water Hg^0 concentrations from the Metzyme cruise transect to a combination of high precipitation (2.5–10 times that of adjacent areas) in the ITCZ (5–15°N) and variations in evasion rates due to local wind speeds [*Soerensen et al*., 2014]. The subsurface maximum in Hg^0 we observed at 12°N is located north of the highest measured surface Hg^0 concentrations, 5–8°N [*Soerensen et al*., 2014], and does not persist beyond regions where denitrification is focused (Figure 3). In addition, beneath the mixed layer, maxima in Hg^0 concentrations are not accompanied by differences in THg (Figure 4a). Instead, the Hg^0 dynamics in the intermediate waters appear to be a result of speciation differences rather than differences in net supply of THg above the thermocline.

In contrast to the maximum of Hg^0 at 12°N, the maximum at 15°S appears in waters of relatively high dissolved O_2 concentrations, 164 μM/kg, and no corresponding minimum in N* value (Figure 3). Here net Hg(II) reduction appears independent of denitrification. This Hg^0 maximum in the South Pacific co-occurs with local maxima in both dissolved PO_4^{3-} and NO_3^- (Figure 2) at a depth of 250 m, deeper than light penetration to drive photodemethylation and subsequent Hg(II) reduction. Photochemical processes are thought to dominate reduction in a range of systems, including coastal and open ocean waters [*Monperrus et al*., 2007; *Whalin et al*., 2007; *Qureshi et al*., 2010]. Beneath the euphotic zone, indirect biotic reduction of Hg(II) by common marine bacteria during generation of reactive oxygen has also been hypothesized as a possible mechanism [*Diaz et al*., 2013], but this remains to be tested.

4.2. Fluxes of Mercury in the Central Pacific

As noted, particulate THg fluxes closely agree with modeled fluxes from the mixed layer and are greater than regional wet and dry deposition [*Soerensen et al*., 2014] (Table 4). Particulate THg fluxes are influential for both removal of Hg species through sorption onto sinking organic matter as well as Hg(II) delivery to intermediate waters for methylation [*Sunderland et al*., 2009].

However, given the particulate fluxes of THg, the methylated Hg concentrations are surprising. Despite low particulate THg delivery at 17°N (Table 4), intermediate waters in the North Pacific have substantially higher methylated Hg species concentrations [*Sunderland et al*., 2009] than those measured in Equatorial and South Pacific stations (Table 2) where delivery of THg is greater (Table 3). Likewise, higher particulate THg fluxes were measured at 8°N compared to 17°N despite similar methylated Hg concentrations (Table 4). This indicates that additional inputs, beyond Hg(II) substrate delivery, are required to account for methylated Hg in intermediate waters.

Elevated MeHg concentrations were not linked to total fluorescence, a proxy of primary production, in a time series study of MeHg concentrations in Mediterranean waters [*Heimbürger et al*., 2010]. Instead, elevated MeHg was measured in intermediate waters (100–1500 m) during seasonal dominance of nanophytoplankton and picophytoplankton as the environment shifted toward oligotrophy [*Heimbürger et al*., 2010]. The slow sinking rates and great surface/volume ratios of small plankton may increase exposure to Hg(II) for methylation relative to larger plankton in intermediate waters [*Heimbürger et al*., 2010]. As a result, we might expect elevated MeHg concentrations along the Metzyme transect to occur in the oligotrophic subtropical gyres where heterotrophic activity may promote methylation despite low Hg(II) export flux. However, MeHg concentrations were focused in intermediate waters beneath the equatorial upwelling region rather than gyres (Figure 5).

Recently, we indexed the anthropogenic input of mercury into the global ocean to that of anthropogenic CO_2 to estimate the extent of anthropogenic marine Hg increases [*Lamborg et al*., 2014]. Our results indicate a 3.5-fold increase in surface THg concentrations compared to preanthropogenic levels [*Lamborg et al*., 2014]. The increases in THg:C ratios of sinking particles from 60 m to 500 m (Table 3) suggest that THg is preferentially transported to depth by sinking particles relative to organic carbon. However, we cannot evaluate whether such trends are consistent across ocean basins due to the scarcity of sinking particle Hg data.

Table 6. Dissolved Hg Species Concentrations Versus Apparent Oxygen Utilization[a]

Region	THg Versus AOU	r^2	MeHg Versus AOU	r^2	DMHg Versus AOU	r^2	MMHg Versus AOU	r^2
All Stations	2.7e–3 (108)	0.67	4.4e–4 (87)	0.49	2.1e–4 (98)	0.41	2.3e–4 (88)	0.37
17°N–8°N	3.6e–4 (34)	0.07	1.1e–4 (26)	0.08	5.8e–5 (34)	0.09	1.2e–4 (26)	0.10
4°N–3.5°S	2.4e–3 (30)	0.47	5.9e–4 (26)	0.41	3.0e–4 (29)	0.35	3.6e–4 (27)	0.35
6°S–15°S	3.2e–3 (44)	0.89	2.8e–4 (35)	0.69	2.7e–4 (35)	0.85	1.3e–5 (35)	0.05

[a]Results of linear regression and coefficients of determination for dissolved Hg speciation versus calculated AOU from 150 to 1500 m for regions of the Central Pacific. Sample numbers are shown in parentheses. MeHg is methylated Hg, the combined sum of DMHg and MMHg.

4.3. Methylated Mercury and Oxygen Utilization

The current understanding of net Hg(II) methylation implicates low-oxygen waters as regions of methylation due to microbial activity and Hg(II) substrate availability from the remineralization of organic matter [*Cossa et al.*, 2009; *Sunderland et al.*, 2009]. As a result, the regression coefficient of methylated Hg ([MMHg] + [DMHg]) concentrations versus extent of AOU in pmol methylated Hg/μmol AOU has been interpreted to represent the methylation capacity of water masses [*Cossa et al.*, 2009; *Heimbürger et al.*, 2010]. From our measurements, this methylation capacity is low in intermediate waters (150–1500 m) for all stations, 0.0004 ($r^2 = 0.49$; $n = 87$; $p < 0.001$; Table 6), an order of magnitude less than that measured in the North Pacific [*Sunderland et al.*, 2009], the Southern Ocean [*Cossa et al.*, 2011], and the Mediterranean Sea [*Cossa et al.*, 2009; *Heimbürger et al.*, 2010].

Closer inspection of the methylation capacity of Pacific waters indicates regional variability. At the 17°N and 8°N station, methylated Hg concentrations are not linearly correlated with AOU ($p > 0.1$) (Table 6). The lack of methylation in intermediate waters appears directly related to the loss of substrate for methylation due to reduction of Hg(II) to Hg^0 in subsurface waters (discussion above; Figure 3). The methylation capacity increases, but is variable, in Equatorial waters, 0.0006 ($r^2 = 0.41$; $n = 26$; $p < 0.05$). South of the equator, the methylation capacity decreases, 0.0003 ($r^2 = 69$; $n = 35$; $p < 0.001$). In addition to the low methylation capacity determined from methylated Hg concentrations, the percentage of THg as methylated Hg does not change significantly with AOU ($p > 0.1$; Figure 7). As a result, methylation appears to be a steady state process in Equatorial and South Pacific waters rather than one that is promoted by organic matter remineralization.

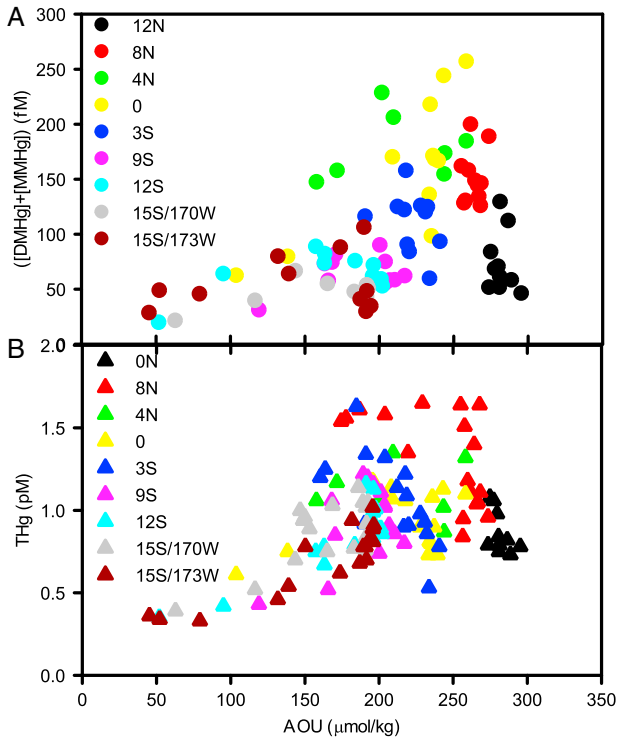

Figure 7. Sums of methylated Hg (measured separately as DMHg and MMHg) concentrations in intermediate waters (150–1000 m) are shown versus AOU (a). Methylated Hg concentrations increase linearly with AOU at all intermediate depths and clump by station, most noticeably in the North Pacific. Concentrations of THg versus AOU (b) show a similar relationship as that of MMHg versus AOU.

In a refinement of the observed relationship between remineralization and Hg(II) methylation, *Sunderland et al.* [2009] found a significant correlation between methylated Hg concentrations and the organic carbon remineralization rate (OCRR), a value that incorporates the age of water masses into estimates of organic matter remineralization

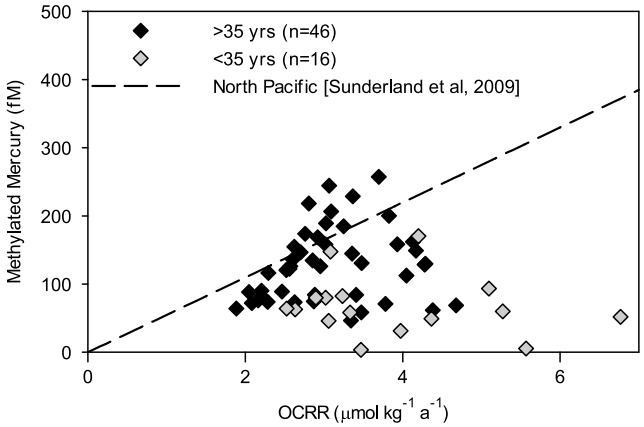

Figure 8. Combined concentrations of dissolved DMHg and MMHg from distinct measurements made between 150 and 1000 m are shown versus organic carbon remineralization rates measured from CFC-12 water mass ages. Since the accuracy of CFC-based water mass ages is limited to 35 years [*Feely et al*., 2004], values for which CFCs are most accurate (grey) are distinguished from those that are older than 35 years (black). No correlation between methylated Hg and OCRR is observed in the Central Pacific which contrasts the relationship (dashed line) observed in the North Pacific, where methylated Hg = 55 ± 15 × (OCRR) [*Sunderland et al*., 2009].

[*Feely et al*., 2004]. The extension of this correlation has important implications for our mechanistic understanding of methylation in the marine water column. Such a relationship implies that low-oxygen waters are poised to methylate Hg(II) substrate as it becomes available (i.e., is released from particulate organic matter).

In contrast to North Pacific waters [*Sunderland et al*., 2009], we observed no significant relationship, either by station or from all data, between intermediate water (150–1000 m) methylated Hg concentrations and OCRR from in Central Pacific waters ($n = 62$; $p > 0.1$) (Figure 8). Although the particulate supply of THg out of the mixed layer is lower in the South Pacific relative to the North Pacific [*Soerensen et al*., 2014], the corresponding lower productivity of these waters would consequently lower the MeHg in South Pacific waters. As a result, it appears that there are differences in the controls on methylation between the North and South Pacific. Unlike the North Pacific Intermediate Waters sampled by *Sunderland et al*. [2009], Central Pacific waters appear to have decreased capacity to methylate Hg(II) released during organic matter remineralization. This could reflect limitation of mercury methylation by some specific compound, either a component of seawater or a requirement for microbial methylation activity, or decreased availability of THg substrate. These regions may therefore be important for the determination of factors that influence marine methylation.

The breakdown of the relationship between methylation and OCRR between the North and South Pacific is important for global estimates of marine methylation capacity, such as the development of global models. Recent work in the Arctic has utilized the North Pacific relationship between methylated Hg and OCRR to distinguish local methylated Hg production from external sources of methylated Hg [*Wang et al*., 2012]. While the strong relationship observed between OCRR and methylated Hg has been observed both in the North Pacific [*Sunderland et al*., 2009] and the Southern Ocean [*Cossa et al*., 2011] and may support the use of OCRR in specific regions, our results suggest that OCRR is not an appropriate parameterization of methylated Hg production across all ocean basins.

4.4. Temporal Trends in Dissolved Mercury Speciation

Measurements of Hg speciation, especially MMHg, have the potential to inform our understanding of how increases in marine Hg concentrations will influence incorporation of MMHg into marine food webs. Although full Hg speciation was first measured in the Equatorial and South Pacific [*Kim and Fitzgerald*, 1986, 1988; *Gill and Fitzgerald*, 1988; *Mason and Fitzgerald*, 1990, 1991, 1993], there have been no subsequent published measurements of Hg in these waters over the past two decades. In addition, poor intercomparibility of open ocean Hg measurements may confound estimates of temporal changes of Hg species. Previous intercalibration efforts among several laboratories for THg in seawater have revealed intercomparability of only 40%, with deviations likely due to inadequate calibration [*Lamborg et al*., 2012]. Therefore, careful consideration of the Hg analysis workflow was taken in accordance with protocols suggested for U.S. GEOTRACES expeditions [*Lamborg et al*., 2012].

Previous ranges of Equatorial THg (measured as HgR) were 0.47–4.94 pM [*Mason and Fitzgerald*, 1993]. However, more recent summaries of basin-scale differences in THg values have reported ranges of 1–2 pM

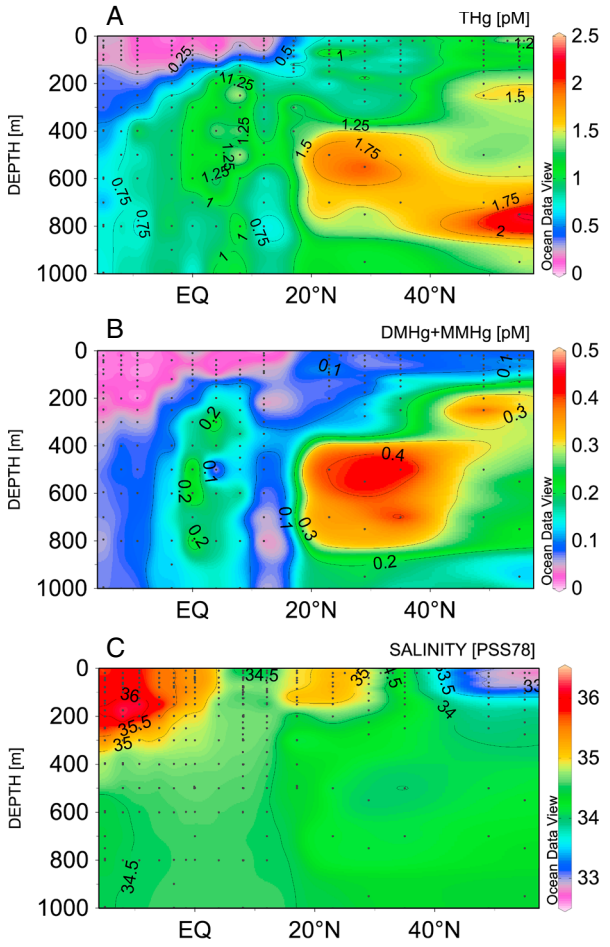

Figure 9. Dissolved THg and MeHg from the CLIVAR P16N section in the North Pacific and the Metzyme cruise in the Tropical Pacific. (a) THg concentrations and (b) methylated Hg in intermediate waters from the CLIVAR P16N section [*Sunderland et al.*, 2009] and continuing southwest with Metzyme stations. THg concentrations reveal that the southward extent of North Pacific Intermediate Water is limited to ~15°N. Like THg, methylated Hg shows distinct distributions in the equatorial Pacific compared to those of the North Pacific Intermediate Water mass as indicated by salinity values (c).

[*Mason et al.*, 2012], which may reflect reevaluation of historical data. Comparison between the original data from 1990 shows our measured THg concentrations in the upper water column are lower than those in nearest stations reported by *Mason and Fitzgerald* [1993]. Above the thermocline (200 m) in waters south of 4°N, we observed an average of 0.25 ± 0.14 pM THg, which is significantly lower (<0.001) than the average observed in 1990, 1.59 ± 1.14 pM (Stations 4 and 6–9) [*Mason and Fitzgerald*, 1993]. Below the thermocline, the average THg concentrations (0.75 ± 0.21 pM) were also lower than those measured in 1990 (1.27 ± 0.47 pM) [*Mason and Fitzgerald*, 1993].

In addition to differences in concentration, the shape of concentration profiles differs in 2011 compared with those collected in 1990. A clear maximum in THg at 500 m was observed by Mason and Fitzgerald in the South Pacific waters between 0 and 10°S and 140°W and 170°E [*Mason and Fitzgerald*, 1993] (Stations 4 and 6–9). This feature is absent from the depth profiles of THg from 6°S and 9°S, which fall within the area sampled by Mason and Fitzgerald (Figure 4). Instead, the shape of the profiles measured by Mason and Fitzgerald most closely resembles our profiles from Station 1 to Station 5 where a clear maximum is observed at depths of net remineralization (Figure 4a). However, despite the similarities in profile shape, our data show a much lower THg concentrations in the upper 200 m (<2 pM). Together, our results reveal no temporal increases in THg in the Equatorial or South Pacific over the past 30 years.

The lack of a measured increase in THg in Equatorial waters is surprising given the significant increase in North Pacific THg concentrations reported between the North Pacific Intergovernmental Oceanographic Commission (IOC) cruise in 2002 [*Laurier et al.*, 2004] and those measured from similar latitudes during the CLIVAR 2006 cruise [*Sunderland et al.*, 2009] and recently implied through reexamination of Hg concentrations reported for yellowfin tuna caught near Hawai'i [*Kraepiel et al.*, 2003; *Choy et al.*, 2009; *Drevnick et al.*, 2015]. We did not reoccupy sites measured by CLIVAR or IOC and therefore cannot determine the extent of subsequent increases or confirm IOC concentrations in dissolved THg in the North Pacific. However, given the water mass differences of our sampling locations, we are able to place spatial constraints on such increases.

Similarities in the dissolved THg profile of 17°N compared to that of Station 45 of the CLIVAR P16N cruise (Figure 8) [*Sunderland et al.*, 2009] suggest that the same processes determine the Hg distributions at both locations. The salinity data from the upper 1000 m at 17°N are consistent with water masses sampled at Station 45 of the CLIVAR P16N cruise (Figure 9) [*Sunderland et al.*, 2009]. However, the THg concentrations we measured at 17°N station fall between those measured during IOC (Station 9, 22.45°N, 158°W) and CLIVAR P16N (Station 45, 23°N, 152°W) (Figure 9). These intermediate values contrast to the approximately

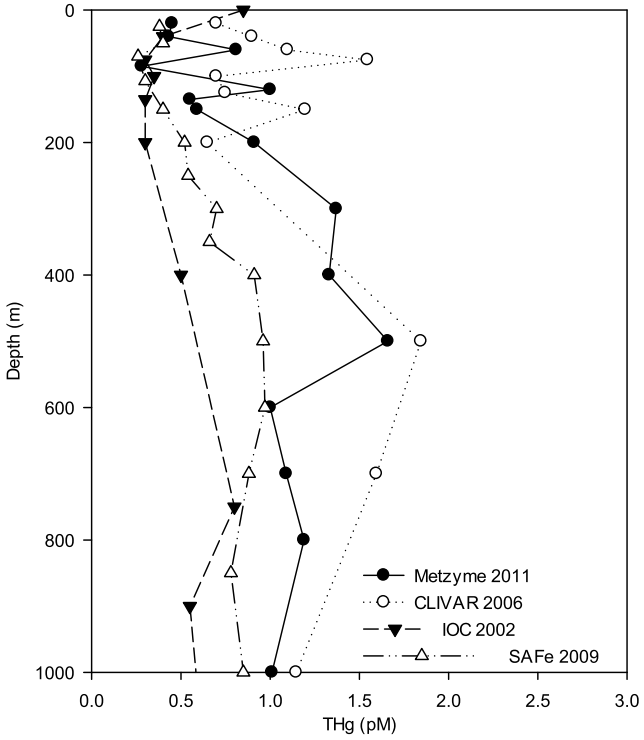

Figure 10. Dissolved THg concentrations in the water column measured at three sites in the North Pacific over a 9 year span. The International Oceanographic Commission 2002 (IOC 2002) data from Station Aloha [*Laurier et al*., 2004], the CLIVAR P16N 2006 data from Station 45 [*Sunderland et al*., 2009], SAFe 2009 station data [*Hammerschmidt and Bowman*, 2012], and the northernmost Metzyme station.

twofold increase that was found to occur in the North Pacific from comparison of all stations of the IOC and CLIVAR P16N THg data [*Sunderland et al*., 2009]. As a result, we conclude that the temporal increase observed between 2002 and 2006 either did not persist southward to 17°N or has not continued in the subsequent 5 year period between measurements in this region to an extent that is discernable. Regardless, due to the close relationship between the salinity and THg profiles of both our data and that of the CLIVAR P16N cruise (Figure 9), our data suggest that the rate of increase in THg concentrations reported by *Sunderland et al*. [2009] is limited to the North Pacific Intermediate Water (NPIW), a specific water mass that extends southward at ~155°W only to ~20°N [*Talley*, 1993]. As a result, we would not expect to see the impact of high THg or methylated Hg from NPIW to persist southward along our Metzyme cruise track. Indeed, the Central and Equatorial Pacific appear to be a region with distinct Hg cycling compared to the North Pacific (Figure 9), and this implies that the impact that anthropogenic Hg emissions have had on fish Hg concentrations could be regional due to various oceanographic effects. For example, we recently suggested that the thermocline waters of the Central and Equatorial Pacific Ocean were relatively free of anthropogenic Hg in contrast to other nearby water masses through the use of remineralized P as an index [*Lamborg et al*., 2014]. The cause for this is unknown but suggests that these waters are distinct with respect to Hg cycling from those of farther north.

In addition to the latitudinal limits on areas of enrichment of THg in the North Pacific, previous studies support a limited longitudinal extent of North Pacific enrichment. Concentrations of THg have been found to vary by up to factor of 2 in NPIW (S = 34) between stations occupied during the CLIVAR P16N cruise and the SAFe site, which are separated by ~1000 km (Figure 10) [*Sunderland et al*., 2009; *Hammerschmidt and Bowman*, 2012]. The large variations in THg concentrations apparent over small spatial scales must be incorporated into basin-scale estimates of Hg enrichment.

Like THg concentrations, methylated Hg concentrations in the Equatorial and South Pacific are low relative to those previously measured in the North Pacific [*Sunderland et al*., 2009]. The general decrease in dissolved THg, DMHg, and MMHg from the North Pacific toward the South Pacific follows increasing trends in dissolved oxygen concentrations. However, given the supply of particulate matter to intermediate waters, low DMHg and MMHg concentrations do not appear to be the result of limited THg supply in regions of net remineralization. Instead, additional factors beyond bulk THg substrate supply appear to limit methylation south of the North Pacific Gyre (Figure 8). Methylation of THg appears limited in waters despite sufficient organic matter remineralization, perhaps due to variations in its availability. In addition, in extremely low oxygen waters, denitrification causes a decrease in DMHg and MMHg concentrations either by reduction of Hg(II) substrate or by demethylation and subsequent reduction of methylated Hg. Such processes must be taken into account when considering how changes in Hg emissions and ocean chemistry will ultimately impact MMHg bioaccumulation over time.

Acknowledgments
Financial support for this study was provided by the National Science Foundation in a grant from the Chemical Oceanography Program (OCE-1031271) to C.H. Lamborg and M.A. Saito and a Graduate Student Fellowship to K.M. Munson. We thank Erin Bertrand, Rene Boiteau, Tyler Goepfert, Nick Hawco, Dawn Moran, and David Wang for their assistance in water sampling, filtration, and pump deployment. We also thank Vic Polidoro, Trevor Young, and the crew of the R/V *Kilo Moana* for making sample collection possible. Thanks to Paul Henderson of WHOI's Nutrient Analytical Facility for CHN analyses. We thank Anne Soerensen and Elsie Sunderland for providing electronic versions of published data, Bill Jenkins and John Bullister for advice and providing water mass ages, and Anne Soerensen and Lars-Eric Heimbürger for reviews. Full speciation data, formatted for Ocean Data View [*Schlitzer*, 2004], are available in the supporting information Table S1.

References

Blum, J. D., B. N. Popp, J. C. Drazen, C. A. Choy, and M. W. Johnson (2013), Methylmercury production below the mixed layer in the North Pacific Ocean, *Nat. Geosci.*, *6*, 879–884.

Bowman, K. L., and C. R. Hammerschmidt (2011), Extraction of monomethylmercury from seawater for low-femtomolar determination, *Limnol. Oceanogr. Methods*, *9*, 121–128.

Bryden, H. L., and E. C. Brady (1985), Diagnostic model of the three-dimensional circulation in the upper Equatorial Pacific Ocean, *J. Phys. Oceanogr.*, *15*, 1255–1273.

Choy, C. A., B. N. Popp, J. J. Kaneko, and J. C. Drazen (2009), The influence of depth on mercury levels in pelagic fishes and their prey, *Proc. Natl. Acad. Sci. U.S.A.*, *106*(33), 13,865–13,869.

Cossa, D., J.-M. Martin, K. Takayanagi, and J. Sanjuan (1997), The distribution and cycling of mercury species in the western Mediterranean, *Deep Sea Res., Part II*, *44*, 721–740.

Cossa, D., B. Averty, and N. Pirrone (2009), The origin of methylmercury in open Mediterranean waters, *Limnol. Oceanogr.*, *54*, 837–844.

Cossa, D., L.-E. Heimbürger, D. Lannuzel, S. R. Rintoul, E. C. V. Butler, A. R. Bowie, B. Averty, R. J. Watson, and T. Remenyi (2011), Mercury in the Southern Ocean, *Geochim. Cosmochim. Acta*, *75*, 4037–4052.

Deutsch, C., N. Gruber, R. M. Key, and J. L. Sarmiento (2001), Denitrification and N_2 fixation in the Pacific Ocean, *Global Biogeochem. Cycle*, *18*, GB4012, doi:10.1029/2000GB001291.

Diaz, J. M., C. M. Hansel, B. M. Voelker, C. M. Mendes, P. F. Andeer, and T. Zhang (2013), Widespread production of extracellular superoxide by heterotrophic bacteria, *Science*, *340*, 1223–1226.

Drevnick, P. E., C. H. Lamborg, and M. J. Horgan (2015), Increase in mercury in Pacific yellowfin tuna, *Environ. Toxicol. Chem.*, doi:10.1002/etc.2883.

Feely, R. A., C. L. Sabine, R. Schlitzer, J. L. Bullister, S. Mecking, and D. Greeley (2004), Oxygen utilization and organic carbon remineralization in the upper water column of the Pacific Ocean, *J. Oceanogr.*, *60*, 45–52.

Food and Agriculture Organization of the United Nations (2013), FAO Yearbook, Fishery and Aquaculture Statistics, 2011 Rome: FAO Statistics and Information Service of the Fisheries and Aquaculture Department.

Garcia, H. E., and L. I. Gordon (1992), Oxygen solubility in seawater: Better fitting equations, *Limnol. Oceanogr.*, *37*(6), 1307–1312.

Gill, G. A., and K. W. Bruland (1987), Mercury in the northeast Pacific, *Eos Trans. AGU*, *68*, 173.

Gill, G. A., and W. F. Fitzgerald (1988), Vertical mercury distributions in the oceans, *Geochim. Cosmochim. Acta*, *52*, 1719–1728.

Gilmour, C. C., M. Podar, A. L. Bullock, A. M. Graham, S. D. Brown, A. C. Somenahally, A. Johs, R. A. Hurt Jr., K. L. Bailey, and D. A. Elias (2013), Mercury methylation by novel microorganisms from new environments, *Environ. Sci. Technol.*, *47*, 11,810–11,820.

Gordon, L. I., J. C. Jennings Jr., A. A. Ross, and J. M. Krest (1994), A suggested protocol for continuous flow analysis of seawater nutrients (phosphate, nitrate, nitrite, and silicic acid) in the WOCE Hydrographic Program and the Joint Global Ocean Fluxes Study. WHIP Office Report 91–1. Revision 1, Nov. 1994.

Gruber, N., and J. L. Sarmiento (1997), Global patterns of marine nitrogen fixation and denitrification, *Global Biogeochem. Cycle*, *11*, 235–266.

Hammerschmidt, C. R., and K. L. Bowman (2012), Vertical methylmercury distributions in the subtropical North Pacific Ocean, *Mar. Chem.*, *132–133*, 77–82.

Heimbürger, L.-E., D. Cossa, J.-C. Marty, C. Migon, B. Averty, A. Dufour, and J. Ras (2010), Methyl mercury distributions in relation to the presence of nano and picophytoplankton in an oceanic water column (Ligurian Sea, North-western Mediterranean), *Geochim. Cosmochim. Acta*, *74*, 5549–5559.

Horvat, M., J. Kotnik, M. Logar, V. Fajon, T. Zvonaric, and N. Pirrone (2003), Speciation of mercury in surface and deep-sea waters in the Mediterranean Sea, *Atmos. Environ.*, *37*, S93–S108.

Jimenez-Moreno, M., V. Perrot, V. N. Epov, M. Monperrus, and D. Amouroux (2013), Chemical kinetic fractionation of mercury during abiotic methylation of Hg(II) by methylcobalamin in aqueous chloride media, *Chem. Geol.*, *336*, 26–36.

Khatiwala, S., F. Primeau, and M. Holzer (2012), Ventilation of the deep ocean constrained with tracer observations and implications for radiocarbon estimates of ideal mean age, *Earth Planet. Sci. Lett.*, *325*, 116–125.

Kim, J. P., and W. F. Fitzgerald (1986), Sea-air partitioning of mercury in the Equatorial Pacific Ocean, *Science*, *231*, 1131–1133.

Kim, J., and W. F. Fitzgerald (1988), Gaseous mercury profiles in the tropical Pacific Ocean, *Geophys. Res. Lett.*, *15*, 40–43, doi:10.1029/GL015i001p00040.

Kraepiel, A. M. L., K. Keller, H. B. Chin, E. G. Malcolm, and F. M. M. Morel (2003), Sources and variations of mercury in tuna, *Environ. Sci. Technol.*, *37*(24), 5551–5558.

Kritee, K., J. D. Blum, M. W. Johnson, B. A. Bergquist, and T. Barkay (2007), Mercury stable isotope fractionation during reduction of Hg(II) to Hg^0 by mercury resistant microorganisms, *Environ. Sci. Technol.*, *41*, 1889–1895.

Lamborg, C. H., K. R. Rolfhus, W. F. Fitzgerald, and G. Kim (1999), The atmospheric cycling and air-sea exchange of mercury species in the South and equatorial Atlantic Ocean, *Deep Sea Res., Part II*, *46*(5), 957–977.

Lamborg, C. H., K. O. Buesseler, and P. J. Lam (2008a), Sinking fluxes of minor and trace elements in the North Pacific Ocean measured during the VERTIGO program, *Deep Sea Res., Part II*, *55*, 1564–1577.

Lamborg, C. H., O. Yigiterhand, W. F. Fitzgerald, P. H. Balcom, C. R. Hammerschmidt, and J. Murray (2008b), Vertical distribution of mercury species at two sites in the Western Black Sea, *Mar. Chem.*, *111*, 77–89.

Lamborg, C. H., C. R. Hammerschmidt, G. A. Gill, R. P. Mason, and S. Gichuki (2012), An intercomparison of procedures for the determination of total mercury in seawater and recommendations regarding mercury speciation during GEOTRACES cruises, *Limnol. Oceanogr. Methods*, *10*, 90–100.

Lamborg, C. H., C. R. Hammerschmidt, K. L. Bowman, G. J. Swarr, K. M. Munson, D. C. Ohnemus, P. J. Lam, L.-E. Heimburger, M. J. A. Rijkenberg, and M. A. Saito (2014), A global ocean inventory of anthropogenic mercury based on water column measurements, *Nature*, *512*, 65–68, doi:10.1038/nature13563.

Laurier, F. J. G., R. P. Mason, G. A. Gill, and L. Whalin (2004), Mercury distributions in the North Pacific Ocean—20 years of observations, *Mar. Chem.*, *90*, 3–19.

Lehnherr, I., V. L. S. Louis, H. Hintelmann, and J. L. Kirk (2011), Methylation of inorganic mercury in polar marine waters, *Nat. Geosci.*, *4*, 298–302, doi:10.1038/ngeo1134.

Mason, R. P., and W. F. Fitzgerald (1990), Alkylmercury species in the Equatorial Pacific, *Nature*, *347*, 457–459.

Mason, R. P., and W. F. Fitzgerald (1991), Mercury speciation in open ocean waters, *Water, Air, Soil Pollut.*, *56*, 779–789.

Mason, R. P., and W. F. Fitzgerald (1993), The distribution and cycling of mercury in the Equatorial Pacific Ocean, *Deep Sea Res., Part I*, *40*(9), 1897–1924.

Mason, R. P., and G.-R. Sheu (2002), Role of the ocean in the global mercury cycle, *Global Biogeochem. Cycle*, *4*, 1093, doi:10.1029/2001GB001440.

Mason, R. P., and K. A. Sullivan (1999), The distribution and speciation of mercury in the south and equatorial Atlantic, *Deep Sea Res., Part II*, *46*, 937–956.
Mason, R. P., F. M. M. Morel, and H. F. Hemond (1995), The role of microorganisms in elemental mercury formation in natural waters, *Air Water Soil Pollut.*, *80*, 775–787.
Mason, R. P., K. R. Rolfhus, and W. F. Fitzgerald (1998), Mercury in the North Atlantic, *Mar. Chem.*, *61*, 37–53.
Mason, R. P., A. I. Choi, W. F. Fitzgerald, C. R. Hammerschmidt, C. H. Lamborg, A. L. Soerensen, and E. M. Sunderland (2012), Mercury biogeochemical cycling in the ocean and policy implications, *Environ. Res.*, *119*, 101–117.
Monperrus, M., E. Tessier, D. Amouroux, A. Leynaert, P. Huonnic, and O. F. X. Donard (2007), Mercury methylation, demethylation and reduction rates in coastal and marine surface waters of the Mediterranean Sea, *Mar. Chem.*, *107*, 49–63.
Munson, K. M., D. Babi, and C. H. Lamborg (2014), Monomethylmercury determination from seawater using ascorbic-acid assisted direct ethylation, *Limnol. Oceanogr. Meth.*, *12*, 1–9, doi:10.4319/lom.2014.12.1.
Noble, A. E., et al. (2012), Basin-scale plumes of cobalt, iron, and manganese emanating from the Benguela-Angola front in the South Atlantic Ocean, *Limnol. Oceanogr.*, *57*, 989–1000.
Pacyna, E. G., J. M. Pacyna, F. Steenhuisen, and S. Wilson (2006), Anthropogenic mercury emission inventory for 2000, *Atmos. Environ.*, *22*, 4048–4063.
Poulain, A. J., S. M. Ni Chadhain, P. A. Ariya, M. Amyot, E. Garcia, P. G. C. Campbell, G. J. Zylstra, and T. Barkay (2007), Potential for mercury reduction by microbes in the high Arctic, *Appl. Environ. Microbiol.*, *73*, 2230–2238.
Qureshi, A., N. J. O'Driscoll, M. Macleod, Y.-M. Neuhold, and K. Hungerbühler (2010), Photoreactions of mercury in surface ocean water: Gross reaction kinetics and possible pathways, *Environ. Sci. Technol.*, *44*, 644–649.
Rodriguez-Gonzalez, P., V. N. Epov, R. Bridou, E. Tessier, R. Guyoneaud, M. Monperrus, and D. Amouroux (2009), Species-specific stable isotope fractionation of mercury during Hg(II) methylation by anaerobic bacteria (*Delsufobulbus propionicus*) under dark conditions, *Environ. Sci. Technol.*, *43*, 9183–9188.
Rolfhus, K. R., and W. F. Fitzgerald (2004), Mechanisms and temporal variability of dissolved gaseous mercury production in coastal seawater, *Mar. Chem.*, *90*, 125–136.
Sarmiento, J. L., and N. Gruber (2006), *Ocean Biogeochemical Dynamics*, 526 pp., Princeton Univ. Press, Princeton, N. J.
Schaefer, J. K., J. Letowski, and T. Barkay (2002), *mer*-mediated resistance and volatilization of Hg(II) under anaerobic conditions, *Geomicrobiol. J.*, *12*, 87–102.
Schlitzer, R. (2004), Ocean data view. [Available at http://odv.awi-bremerhaven.de.]
Soerensen, A. L., E. M. Sunderland, C. D. Holmes, D. J. Jacob, R. M. Yantosca, H. Skov, J. H. Christensen, S. A. Strode, and R. P. Mason (2010), An improved global model for air-sea exchange of mercury: High concentrations over the North Atlantic, *Environ. Sci. Technol.*, *44*, 8574–8580.
Soerensen, A. L., R. P. Mason, P. H. Balcom, D. J. Jacob, Y. Zhang, J. Kuss, and E. M. Sunderland (2014), Elemental mercury concentrations and fluxes in the tropical atmosphere and ocean, *Environ. Sci. Technol.*, *48*, 11,312–11,319.
Strode, S. A., L. Jaegle, N. E. Sellin, D. J. Jacob, R. J. Park, R. M. Yantosca, R. P. Mason, and F. Slemr (2007), Air-sea exchange in the global mercury cycle, *Global Biogeochem. Cycle*, *21*, GB1017, doi:10.1029/2006BG002766.
Sunderland, E. M., D. P. Krabbenhoft, J. W. Moreau, S. A. Strode, and W. M. Landing (2009), Mercury sources, distribution, and bioavailability in the North Pacific Ocean: Insights from data and models, *Global Biogeochem. Cycle*, *23*, GB2010, doi:10.1029/2008GB003425.
Talley, L. D. (1993), Distribution and formation of North Pacific Intermediate Water, *J. Phys. Oceanogr.*, *23*, 517–537.
Talley, L. D., G. L. Pickard, W. J. Emery, and J. H. Swift (2011), *Descriptive Physical Oceanography: An Introduction*, 6th ed., 560 pp., Elsevier, Boston, Mass.
U.S. Environmental Protection Agency (EPA) (1998), *Method 1630: Methyl Mercury in Water by Distillation, Aqueous Ethylation, Purge and Trap, and Cold Vapor Atomic Fluorescence Spectrometry*, US EPA Office of Science and Technology, Washington, D. C.
U.S. Environmental Protection Agency (EPA) (2002), *Method 1631, Revision E: Mercury in Water by Oxidation, Purge and Trap, and Cold Vapor Atomic Fluorescence Spectrometry*, US EPA Office of Science and Technology, Washington, D. C.
Wang, F., R. W. Macdonald, D. A. Armstrong, and G. A. Stern (2012), Total and methylated mercury in the Beaufort Sea: The role of local and recent organic remineralization, *Environ. Sci. Technol.*, *46*, 11,821–11,828.
Whalin, L., E.-H. Kim, and R. P. Mason (2007), Factors influenced the oxidation, reduction, methylation, and demethylation of mercury species in coastal waters, *Mar. Chem.*, *107*, 278–294.